



HAL
open science

Morphogenesis is transcriptionally coupled to neurogenesis during peripheral olfactory organ development

Raphaël Aguillon, Romain Madelaine, Harendra Guturu, Sandra Link, Pascale Dufourcq, Virginie Lecaudey, Gill Bejerano, Patrick Blader, Julie Batut

► To cite this version:

Raphaël Aguillon, Romain Madelaine, Harendra Guturu, Sandra Link, Pascale Dufourcq, et al.. Morphogenesis is transcriptionally coupled to neurogenesis during peripheral olfactory organ development. *Development* (Cambridge, England), 2020, 147 (24), 10.1242/dev.192971 . hal-02368916

HAL Id: hal-02368916

<https://hal.science/hal-02368916>

Submitted on 18 Nov 2019

HAL is a multi-disciplinary open access archive for the deposit and dissemination of scientific research documents, whether they are published or not. The documents may come from teaching and research institutions in France or abroad, or from public or private research centers.

L'archive ouverte pluridisciplinaire **HAL**, est destinée au dépôt et à la diffusion de documents scientifiques de niveau recherche, publiés ou non, émanant des établissements d'enseignement et de recherche français ou étrangers, des laboratoires publics ou privés.



Distributed under a Creative Commons Attribution 4.0 International License

Morphogenesis is transcriptionally coupled to neurogenesis during olfactory placode development

Raphaël Aguillon¹, Romain Madelaine¹, Harendra Guturu², Sandra Link^{3§}, Pascale Dufourcq¹, Virginie Lecaudey^{3&}, Gill Bejerano⁴, Patrick Blader^{1*} and Julie Batut^{1*}

¹ Centre de Biologie du Développement (CBD, UMR5547), Centre de Biologie Intégrative (CBI, FR 3743), Université de Toulouse, CNRS, UPS, 31062, France.

² Department of Electrical Engineering, Stanford University, Stanford, CA 94305, USA.

³ BIOS Centre for Biological Signalling Studies, Albert Ludwigs University of Freiburg, Freiburg im Breisgau, Germany.

⁴ Department of Developmental Biology, Department of Computer Science, Department of Pediatrics, Department of Biomedical Data Science, Stanford University, Stanford, CA 94305, USA.

§ Present address: Universitäts-Herzzentrum Freiburg, Kardiovaskuläre Biologie/AG Moser, Breisacher Straße 33 · 79106 Freiburg, Germany.

& Present address: Goethe-Universität - Campus Riedberg, Institute for Cell Biology and Neuroscience, Department of Developmental Biology of Vertebrates, Max-von-Laue-Straße 13, D-60438 Frankfurt am Main, Germany.

*Correspondence to: patrick.blader@univ-tlse3.fr; julie.batut@univ-tlse3.fr

One Sentence Summary: Neurog1 controls olfactory placode morphogenesis via *cxcr4b*

Abstract

Morphogenesis of sense organs occurs concomitantly with the differentiation of sensory cells and neurons necessary for their function. While our understanding of the mechanisms controlling morphogenesis and neurogenesis has grown, how they are coordinated remains relatively unknown. The earliest wave of neurogenesis in the zebrafish olfactory placode requires the bHLH proneural transcription factor Neurogenin1 (Neurog1). To address whether Neurog1 couples neurogenesis and morphogenesis in this system, we analyzed the morphogenetic behavior of early olfactory neural progenitors. Our results indicate that the oriented movements of these progenitors are disrupted in *neurog1* mutants. Morphogenesis is similarly affected by mutations in the chemokine receptor, *cxcr4b*, making it a potential Neurog1 target gene. We find that Neurog1 directly regulates *cxcr4b* through an E-boxes cluster located just upstream of the *cxcr4b* transcription start site. Our results suggest that proneural transcription factors, such as Neurog1, directly couple distinct aspects of nervous system development.

Results and Discussion

The morphology of sense organs of the head, such as the olfactory epithelium and retina, are exquisitely adapted for detecting specific stimuli. Concomitant with the morphogenetic movements that sculpt these structures during development, cell types are specified that will participate in their function either by detecting specific stimuli or transmitting sensory information to the brain. There is a growing literature concerning the molecular mechanisms controlling morphogenesis and specification of different cell types in sensory organs. Whether morphogenesis and cell fate specification are coupled molecularly during the development of these organs, on the other hand, is largely unexplored.

Neurogenesis in the developing zebrafish olfactory placode occurs in two distinct waves, with both requiring the proneural gene *neurog1*, which encodes a bHLH transcription factor (Blader et al., 1997; Madelaine et al., 2011). Concomitant with the earliest wave of neurogenesis in the developing olfactory placode, morphogenetic

movements shape placodal progenitors and newly born neurons into a rudimentary cup (Whitlock and Westerfield, 2000; Miyasaka et al., 2007; Breau et al., 2017). We hypothesized that in parallel to its role in olfactory neurogenesis *Neurog1* is ideally placed to control the cell movements that underlie morphogenesis of the olfactory cup, thus coupling morphogenesis and neurogenesis. To address this possibility, we analyzed morphogenesis of the olfactory cup by time-lapse imaging *neurog1* mutant or wild-type embryos carrying a *Tg(-8.4neurog1:gfp)* transgene (Golling et al., 2002; Blader et al., 2003); this transgene recapitulates the expression of endogenous *neurog1* in the developing placode/cup and can be used as a short-term lineage label for the progenitors of early olfactory neurons, referred to hereafter as EON (Madelaine et al., 2011; Breau et al., 2017). As recently described by Breau and colleagues, we found that EON reach their final position in wild-type embryos by converging towards a point close to the center of the future cup (as represented in Figure 1A; (Breau et al., 2017)). Considering overall antero-posterior (AP) length of the placode, this convergence appears to happen quickly between 12 and 18 hours post-fertilization (hpf), after which it slows (Figure S1A,B). In *neurog1^{hi1059}* mutants, we observed a delay in convergence, which translates into a longer AP length spread of EON than seen in wild-type embryos (Figure S1B). This delay is overcome, however, with the final cup in *neurog1^{hi1059}* mutant embryos attaining AP length of control embryos around 27 hpf (Figure S1B).

To assess the morphogenetic phenotype of *neurog1^{hi1059}* mutant embryos at cellular resolution, we injected synthetic mRNAs encoding Histone2B-RFP (H2B-RFP) into *Tg(-8.4neurog1:gfp)* transgenic embryos, which were again imaged from 12 to 27 hpf. Morphogenetic parameters of individual EON located in the anterior, middle and posterior thirds of the *neurog1:GFP+* population were then extracted from datasets generated by manually tracking H2B-RFP positive nuclei. The position of each tracked EON was then plotted according to their medio-lateral (X) and (Y) position. As for the global analysis, the behavior we observe for single EON in control embryos largely recapitulates those already reported (Figure 1B; (Breau et al., 2017)). Comparing the behavior of EON in *neurog1^{hi1059}* mutants and siblings, we found that whereas EON in the middle and posterior regions of mutant placodes migrate similarly to their wild-type

counterparts, the migratory behavior of anterior EON is profoundly affected in *neurog1*^{hi1059} mutant embryos from 12 to 18 hpf (Figure 1B,C and Figure S2A); morphogenetic movements of individual skin cells showed no obvious differences in control versus *neurog1* mutants suggesting that the effect is specific to EON (Figure S3). Principal component analysis (PCA) of the morphometric datasets confirmed that the major difference between olfactory placode morphogenesis in control and *neurog1*^{hi1059} mutant embryos (PC1) lies in the migratory behavior of anterior EON along the AP axis; PCA revealed a more subtle difference in migration of the middle EON population along the same axis (Figure 1D and Figure S2B) and between the posterior EON populations along the medio-lateral axis (Figure S2B). These migratory defects are not due to a decrease in cell mobility as EON in *neurog1* mutants displayed increase displacement over time compare to controls (Figure S1C,D); little or no difference was detected in the displacement of skin cells between control and *neurog1*^{hi1059} mutant embryos (Figure S1C,E). Taken together, our results indicate that Neurog1 is required for an early phase of morphogenesis of the olfactory placode.

The chemokine receptor *Cxcr4b* and its ligand *Cxcl12a* (also known as *Sdf1a*) have been implicated in olfactory placode morphogenesis in the zebrafish (Miyasaka et al., 2007). To address whether the behavior of EON in *neurog1*^{hi1059} mutants resembles that caused when the activity of this guidance receptor/ligand pair is abrogated, we analyzed the morphogenetic parameters of EON migration in *cxcr4b*^{t26035} and *cxcl12a*^{t30516} mutants (Knaut et al., 2003; Valentin et al., 2007). As previously reported, olfactory placodes of embryos lacking *Cxcr4b* or *Cxcl12a* function display convergence defects, highlighted by an increase in the AP length of the cup relative to controls (Figure S4A; (Miyasaka et al., 2007)). Analysis of the behavior of individual cells in *cxcr4b*^{t26035} and *cxcl12a*^{t30516} mutant embryos indicates that defects in EON migration are largely restricted to the anterior cohort of EON (Figure 2A,B and Figure S5A,B); EON show increased displacement over time in both *cxcr4b*^{t26035} and *cxcl12a*^{t30516} mutants (Figure S4B,C) and no difference is apparent in the behavior of skin cells in either mutant relative to wild-type siblings (Figure S4B,D and S6). A combined PCA of morphometric datasets from anterior EON of *neurog1*^{hi1059}, *cxcr4b*^{t26035} and *cxcl12a*^{t30516} mutants confirms that the major difference in EON behavior lies in their displacement

along the AP axis (PC1; Figure 2C). Finally, unbiased clustering of the PCA analysis reveals that there is more resemblance in the behavior of anterior EON between the three mutants than between any single mutant and controls (Figure 2D).

The similarity between the migration phenotype of EON in *neurog1*^{hi1059}, *cxcr4b*^{t26035} and *cxcl12a*^{t30516} mutant embryos suggests that the proneural transcription factor and the receptor/ligand couple act in the same pathway. To determine if the expression of either the receptor or its ligand are affected in the absence of Neurog1, we assessed their expression in *neurog1*^{hi1059} mutant embryos. We found that *cxcr4b* expression is dramatically reduced or absent in EON progenitors at 12 and 15 hpf in this context (Figure 3A); the expression of *cxcr4b* recovers in *neurog1*^{hi1059} mutant embryos from 18 hpf, a stage at which we have previously reported that the expression of a second bHLH proneural gene, *neurod4*, also becomes Neurog1-independent (Figure 3A; Madelaine et al., 2011). Contrary to *cxcr4b*, the expression of *cxcl12a* is unaffected in *neurog1*^{hi1059} mutant embryos at all stages analyzed (Figure 3B). Taken together, these results suggest that the EON migration phenotype in *neurog1*^{hi1059} mutant embryos results from the lack of Cxcr4b during the early phase of olfactory cup morphogenesis.

If the absence of early *cxcr4b* expression in the olfactory placodes of *neurog1*^{hi1059} mutants underlies the morphogenesis defects, we hypothesized that restoring *cxcr4b* expression should rescue these defects. To test this, we generated a transgenic line where expression of the chemokine receptor is controlled by a -8.4 kb fragment of genomic DNA responsible for *neurog1* expression in EON, *Tg(-8.4neurog1:cxcr4b-mCherry)*, and introduced it into the *neurog1*^{hi1059} mutant background (Blader et al., 2003; Madelaine et al., 2011). Analysis of the migratory behavior of anterior EON in *neurog1*^{hi1059} mutant embryos carrying the transgene indicates that they display oriented posterior migration similar to wild-type siblings carrying the transgene (Figure 3C,D). The similarity in the behavior of the anterior EON is also evident after PCA analysis (Figure 3E). Here, *neurog1*^{hi1059} mutant cells carrying the transgene cluster primarily with control cells rather than mutant cells lacking the transgene (Figure 3E,F). These data lead us to conclude that Cxcr4b is the predominant downstream effector of Neurog1 during the early phase of olfactory cup morphogenesis.

Finally, we asked whether *cxcr4b* is a direct transcriptional target of Neurog1 by searching for potential Neurog1-dependent cis-regulatory modules (CRM) at the *cxcr4b* locus. Proneural transcription factors bind CANNTG sequences known as E-boxes, which are often found in clusters (Bertrand et al., 2002). We identified 18 E-boxes clusters in the sequences from -100 to +100 kb of the *cxcr4b* initiation codon, but only 1 of these clusters contains more than one of the CA^A/_GATG E-box sequence preferred by Neurog1 (Figure 4A and data not shown; (Madelaine and Blader, 2011)). Coherent with a role for this E-box cluster in the regulation of *cxcr4b* expression, a transgenic line generated using a 35kb fosmid clone that contains this cluster, *TgFOS(cxcr4b:eGFP)*, shows robust expression of GFP in the olfactory cup (Figure 4A,D). To investigate whether this cluster act as a *bona fide* Neurog1-dependent CRM, we performed chromatin immunoprecipitation (ChIP) experiments. In the absence of a ChIP compatible antibody against endogenous zebrafish Neurog1, we chose a strategy based on mis-expression of a Ty1-tagged form of Neurog1. Mis-expression of Neurog1-Ty1 efficiently induces the expression of *deltaA*, a known Neurog1 target, and *cxcr4b* suggesting that tagging Neurog1 does not affect its transcriptional activity and that *cxcr4b* behaves as a Neurog1 target (Figure 4B). We have previously shown that the *deltaA* locus contains two proneural regulated CRMs (Madelaine and Blader, 2011); whereas CRM HI is a Neurog1-dependent CRM, HII underlies regulation of *deltaA* by members of the Ascl1 family of bHLH proneural factors (Hans and Campos-Ortega, 2002; Madelaine and Blader, 2011). We found that ChIP against Neurog1-Ty1 after mis-expression effectively discriminates between the Neurog1-regulated HI and Ascl1-regulated HII CRM at the *deltaA* locus, thus providing a control for the specificity of our ChIP experiments (Figure 4C). Similarly, we were able to ChIP the potential CRM containing the E-box cluster 7 suggesting that this region is also a target for Neurog1 (Figure 4C).

To confirm the importance of the E-box cluster in the regulation of *cxcr4b* expression, we employed a Crispr/Cas9 approach to delete this CRM using a pair of sgRNAs flanking the CRM (Figure S7A). The sgRNA pair efficiently induces deletions in the targeted sequence, as judged by PCR on genomic DNA extracted from injected embryos (Figure S7B). Injection of the sgRNA pair into *TgFOS(cxcr4b:eGFP)*

transgenic embryos caused mosaic disruption of the eGFP expression pattern (Figure 4D). Loss of *TgFOS(cxcr4b:eGFP)* transgene expression is not due to cell death as eGFP-negative cells maintain the expression of the early neuronal marker HuC/D (insert in Figure 4D). Taken together, the results from our ChIP and Cripsr/Cas9 experiments strongly suggest that the CATATG E-box cluster upstream of *cxcr4b* is regulated directly by Neurog1.

In zebrafish, the proneural transcription factor Neurog1 directly regulates the expression of the neurogenic genes *deltaA* and *deltaD* (Hans and Campos-Ortega, 2002; Madelaine and Blader, 2011). We have shown that Neurog1 is required for the development of an early wave of neurons in the olfactory placode (Madelaine et al., 2011). The data presented here show that Neurog1 controls an early phase of morphogenesis of the zebrafish peripheral olfactory sensory organ via its target gene *cxcr4b*. We propose that Neurog1 couples neurogenesis with morphogenesis in this organ via the transcriptional regulation of distinct targets. That members of the Neurog family regulate *Delta1* and *Cxcr4* expression, as well as development the olfactory epithelium in mouse suggests that this role may be conserved (Beckers et al., 2000; Mattar et al., 2004; Shaker et al., 2012).

Acknowledgments

This work was supported by the Centre National de la Recherche Scientifique (CNRS); the Institut National de la Santé et de la Recherche Médicale (INSERM); Université de Toulouse III (UPS); Fondation pour la Recherche Médicale (FRM; DEQ20131029166); Fédération pour la Recherche sur le Cerveau (FRC); and the Ministère de la Recherche. We thank Kristen Kwan and Chi-Bin Chien for providing plasmids of the Tol2kit, Stéphanie Bosch and the Toulouse RIO Imaging platform, and Aurore Laire and Richard Brimicombe for taking care of the fish. We also thank Marie Breau, Magali Suzanne, Christian Mosimann and members of the Blader lab for advice on experiments and comments on the manuscript.

Materials and Methods

Fish Husbandry and lines

Ethics Statement and Embryos: All embryos were handled according to relevant national and international guidelines. French veterinary service and national ethical committee approved the protocols used in this study, with approval ID: A-31-555-01 and APAPHIS #3653-2016011512005922v6.

Fish were maintained at the CBD-CBI zebrafish facility in accordance with the rules and protocols in place. The *neurog1*^{hi1059Tg}, *cxcr4b*^{t26035} and *cxcl12a*^{t30516} mutant lines have previously been described (Golling et al., 2002; Knaut et al., 2003; Valentin et al., 2007), as has the *Tg(-8.4neurog1:gfp)*^{sb1} (Blader et al., 2003). Embryos were obtained through natural crosses and staged according to (Kimmel et al., 1995).

Establishment of new transgenic lines

The *TgFOS(cxcr4b:eGFP)*^{fu10Tg} transgenic line was generated using homologous recombination by replacing the second exon of *cxcr4b* by LynGFP in the Fosmid CH1073-406F3, followed by zebrafish transgenesis (Revenu et al., 2014). The first 5 amino acid encoded by the first exon of *cxcr4b* are fused to LynGFP, preventing targeting to the membrane. The GFP localizes to the cytoplasm in this transgenic line.

The *Tg(-8.4neurog1:cxcr4b-mCherry)* transgene was generated by first cloning the coding region of *cxcr4b* minus its endogenous stop codon in frame upstream of mCherry in pCS2. The resulting *cxcr4b-mCherry* fusion coding sequence was transferred into the middle entry clone, pME, of the Tol2kit developed in the Chien lab (Kwan et al., 2007). The final transgene vector was generated using LR recombination with a previously described *p5'-8.4neurog1* (Madelaine et al., 2011), the *pME-cxcr4b-mCherry*, and the *p3E-polyA* and *pDestTol2pA/pDestTol2pA2* from the Tol2kit (Kwan et al., 2007). The new line was then generated by co-injecting the transgene with mRNA encoding Tol2 transposase into freshly fertilized zebrafish embryos.

In situ Hybridization, Immunostaining and Microscopy

In situ hybridization was performed as previously described (Oxtoby and Jowett, 1993). Antisense DIG-labeled probes for *cxcr4b* and *cxcl12a* (David et al., 2002) were

generated using standard procedures. In situ hybridizations were visualized using BCIP and NBT (Roche) as substrates.

Embryos were immunostained as previously described (Madelaine et al., 2011); primary antibody used was mouse anti-HuC/D (1:500; 16A11, Molecular Probes, USA), which was detected using Alexa Fluor 555 conjugated goat anti-mouse IgG diluted 1/1000: (A-28180, Molecular Probes, USA). Immunolabelings were counterstained with Topro3 (T3605, Molecular Probes, USA). Labeled embryos were imaged using an upright SP8 Leica confocal and analyzed using ImageJ and Imaris 8.3 (Bitplane, Switzerland) software.

Cell tracking in time-lapse confocal datasets

Embryos carrying the *Tg(-8.4neurog1:gfp)* transgene (Blader et al., 2003) were injected with synthetic mRNA encoding an H2B-RFP fusion protein; for analysis of the global behavior of olfactory placode morphogenesis, un-injected embryos were used. Embryos were then grown to 12 hpf at which point they were dechorionated and embedded for imaging in 0.7% low-melting point agarose in embryos medium. A time-lapse series of confocal stacks (1 mm slice/180 mm deep) was generated of the anterior neural plate and flanking non-neural ectoderm on an upright Leica SP8 Confocal microscope using a 25x HC Fluotar water-immersion objective. Acquisitions each 7 min were stopped at 27 hpf, when the olfactory rosette was clearly visible. The lineage of anterior, midline and posterior early olfactory neuron cohorts were subsequently constructed semi-automatically following H2B-RFP of neurog1:GFP+ EON using Imaris 8.3 analysis software (Bitplane, Switzerland); for each of three embryos, two anterior, middle and posterior cells from the left and right olfactory placode were tracked.

Track analysis

Track parameters were extracted from Imaris as Excel files and analyzed using a custom script generated in R (The R Project for Statistical Computing, www.r-project.org). First, tracks were rendered symmetric across the left-right axis for ease of interpretation. Tracks were then color coded according to their genotype and to the phase of migration (early from 12-18 hpf; late from 18-27 hpf) and plotted. Finally, the

mean for each set of tracks was generated using the “RowMeans” function and a plot was generated.

Principal component analysis (PCA) and clustering were performed using the built-in R function “prcomp” from the “FactoMineR” package and the “kmeans” function, from the “stats” package, respectively. Finally, the “barplot” function (“graphics” package) was used to represent either the EON cluster composition or the Skin cluster composition.

Chromatin Immunoprecipitation and qPCR

ChIP experiments were performed as previously described using approximately 300 embryos (12 to 15 hpf) per immunoprecipitation (Wardle et al., 2006). Two to four separate ChIP experiments were carried out with corresponding independent batches of either control un-injected embryos or embryos injected with a synthetic mRNA encoding Neurog1-Ty1; ChIP-grade mouse anti-Ty1 (BB2; Sigma-Aldrich, USA) was used. Primers used for qPCR on ChIPs were:

cxcr4b CATATG cluster fw 5'- CTACATCTAAAAATTGAAAGA-3'

cxcr4b CATATG cluster rev 5'- CAAACCCAACACCCCTACTG-3'

deltaA HI fw 5'- GCGGAATGAACCACCAACTT-3'

deltaA HI rev 5'- GTGTGACTAAAGGTGTATGGGTG-3'

deltaA HII fw 5'- TATTGTGTGCAGGCGGAATA-3'

deltaA HII rev 5'-GTTTGAATGGGCTCCTGAGA-3'.

Reactions were carried out in triplicates on a MyIQ device (Bio-Rad). The specific signals were calculated as the ratio between the signals with the Ty1 antibody and beads alone, and were expressed as percentage of chromatin input.

For qPCR experiments, to determine expression levels of *cxcr4b* and *deltaA* after mis-expression of Neurog1-Ty1, total RNAs were extracted from 20 injected embryos at 15 hpf with the RNeasy Mini Kit (QIAGEN), and reverse-transcribed with the PrimeScript RT reagent kit (Ozyme) according to the supplier's instructions. Q-PCR analyzes were performed on MyIQ device (Bio-Rad) with the SsoFast EvaGreen Supermix (Bio-Rad), according to the manufacturer's instructions. All experiments include a standard curve. Samples from embryos were normalized to the number of

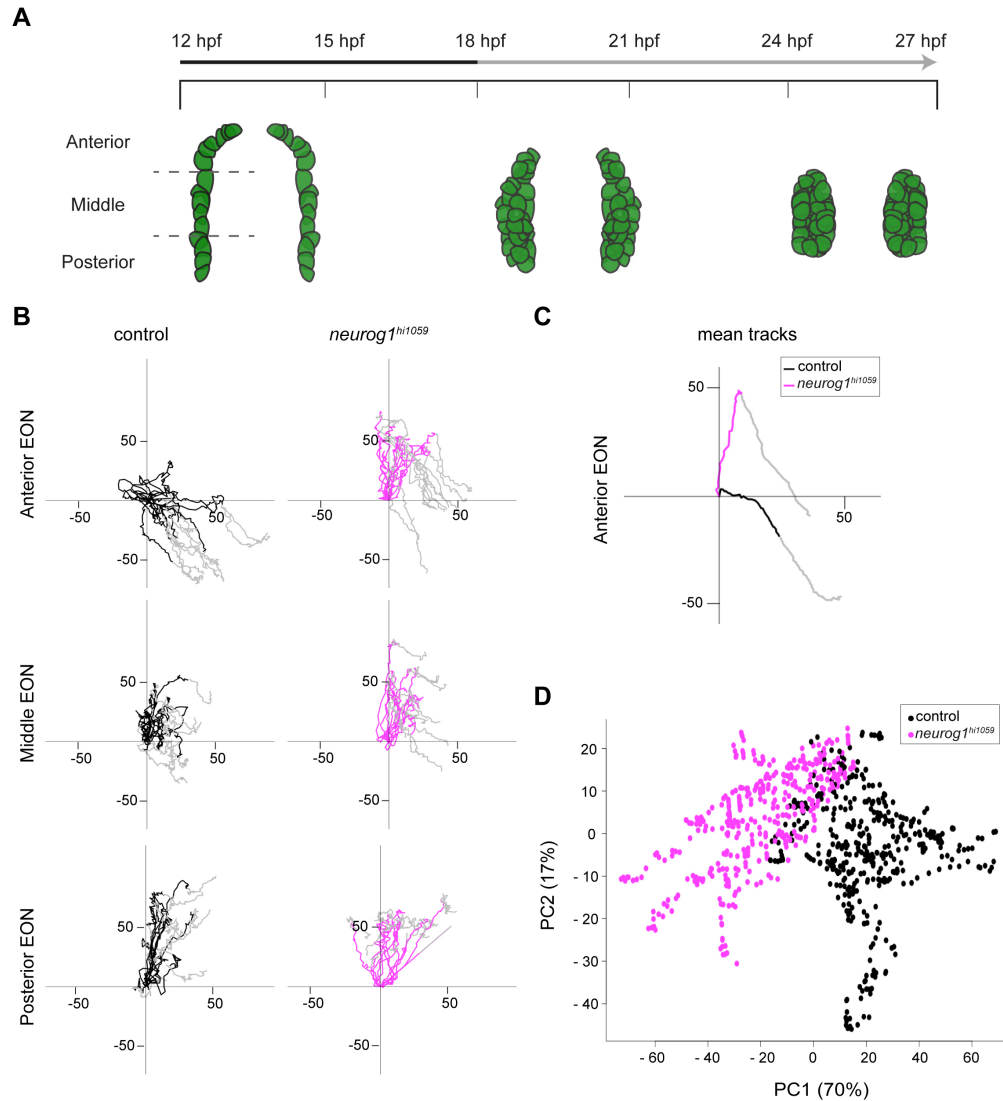
ef1a mRNA copies. Primers for qPCR to determine the expression levels of *cxcr4b* and *deltaA* after mis-expression of Neurog1-Ty1 normalized to the expression of *ef1a* were:
cxcr4b coding fw 5'- GCTGGCATATTTCCACTGCT-3'
cxcr4b coding rev 5'- AGTGCACTGGACGACTCTGA-3'
deltaA coding fw 5'- CGGGTTTACAGGCATGAACT-3'
deltaA coding rev 5'- ATTGTTCTTTTCGTGGCAAG-3'
ef1a fw 5'-GCATACATCAAGAAGATCGGC-3'
ef1a rev 5'-GCAGCCTTCTGTGCAGACTTTG-3'.

Crispr/Cas9 deletion of potential CRM at the *cxcr4b* locus

sgRNA sequences flanking the E-box cluster 7 at the *cxcr4b* locus were designed using the web-based CRISPRscan algorithm (Moreno-Mateos et al., 2015; <http://www.crisprscan.org>). The targeted sequences are 5'-GGCTTATGATGGAGGCGACTGG-3' and 5'-GGCTTGTATTGCCCTTGAGGG-3'; the PAM sequence at the target site are underlined. Templates for the transcription of sgRNAs were generated by PCR following previously described protocols (Nakayama et al., 2014). Injection of sgRNAs was performed as described by Burger and colleagues, using a commercially available Cas9 protein (New England Biolabs). The efficiency of creating deletion after co-injection of the sgRNA pair was determined by PCR on genomic DNA extracted from injected embryos using the following primers:
5'-AACTCGCATTCGGCAAACCTCTC-3'
5'-AAGGGGATAATGAGCAGTCAGC-3'.

While a 500 base-pair PCR fragment is generated from a wild-type locus, an approximately 200 base-pair fragment is amplified if a deletion has been induced.

Figures

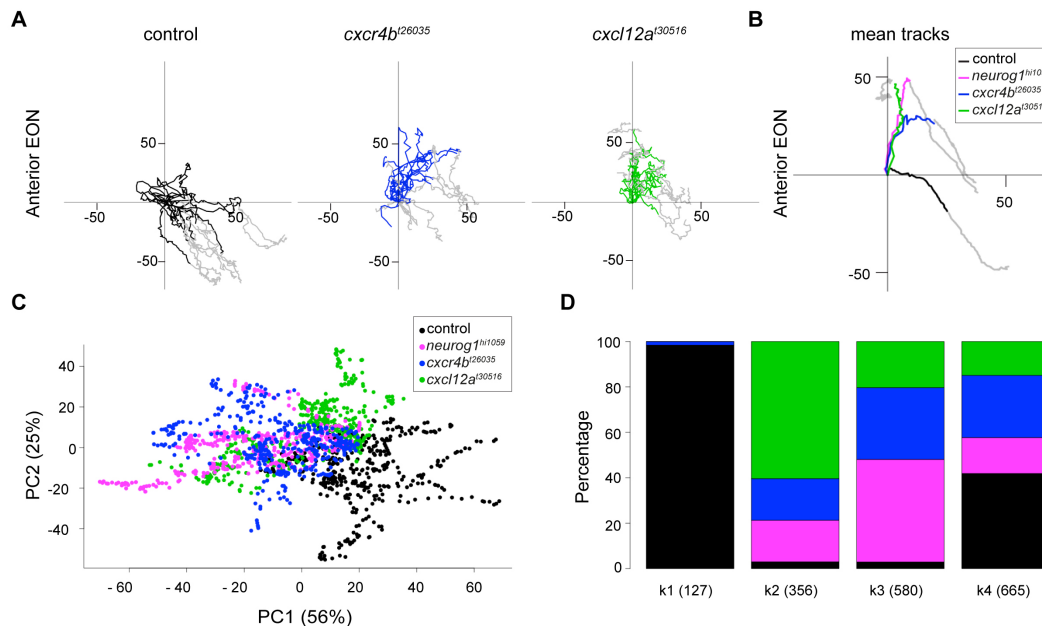


Aguillon et al, Figure 1

Figure 1. Oriented cell movements are affected in *neurog1^{hi1059}* mutant embryos during olfactory placode formation.

(A) Graphic representation of the morphogenesis of olfactory placodes from 12 hpf to 27 hpf showing a dorsal view of the three olfactory stages: olfactory territory (12 hpf), olfactory placode (18 hpf) and olfactory epithelium (24 hpf). Placode EON progenitors are represented in green as visualized with the *Tg(-8.4neurog1:gfp)* transgene. At 12 hpf, the -8.4neurog1:GFP+ placodal domain can be divided in anterior, middle and posterior regions. The early (12-18 hpf; Black) and late (18-27 hpf; Grey) phases of morphogenesis are noted in the time line. (B) Tracks showing migration of EON of control (Black) or *neurog1^{hi1059}* mutant (Magenta) embryos. 12 tracks are represented (2 cells each from the left and right

placodes from 3 embryos) for each of the anterior, middle and posterior domains of the developing placode indicated in (A). The origin of the tracks has been arbitrarily set to the intersection of the X/Y axis and the early (colored) and late (Grey) phases of migration have been highlighted. (C) Mean tracks for anterior EON of control (Black) or *neurog1*^{hi1059} mutant (Magenta) embryos. (D) Pairwise principal component analysis scatterplots of morphogenetic parameters extracted from the datasets corresponding to the tracks in (C). The major difference between control and *neurog1*^{hi1059} mutant embryos (PC1) corresponds to the antero-posterior axis.

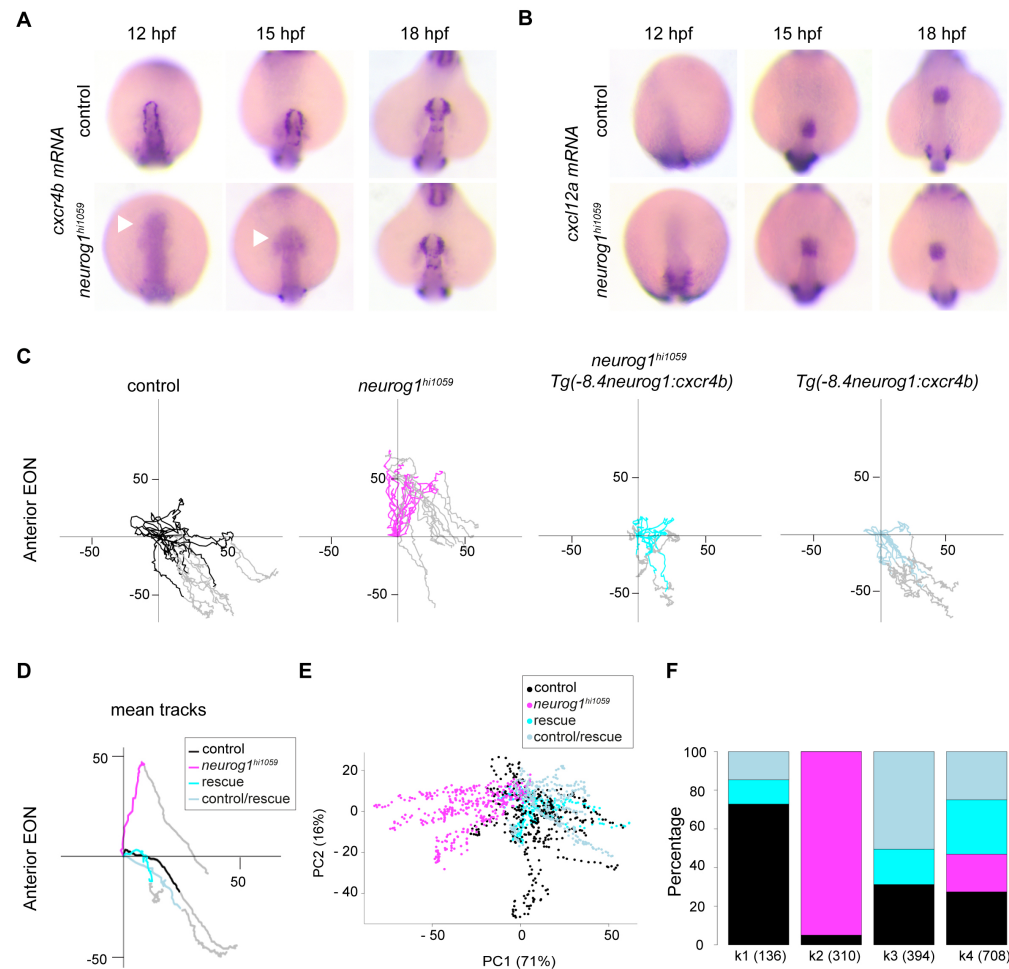


Aguillon et al, Figure 2

Figure 2. Morphogenetic defects in *cxcr4b*^{t26035} and *cxcl12a*^{t30516} mutant embryos resemble those of *neurog1*^{hi1059}.

(A) Tracks showing migration of anterior EON from control (Black), *cxcr4b*^{t26035} (Blue) and *cxcl12a*^{t30516} (Green) embryos. 12 anterior tracks are represented (2 cells each from the left and right placodes from 3 embryos). The origin of the tracks has been arbitrarily set to the intersection of the X/Y axis and the early (colored) and late (Grey) phases of migration have been highlighted. (B) Mean tracks showing migration of anterior EON of control (Black), *neurog1*^{hi1059} (Magenta), *cxcr4b*^{t26035} (Blue) and *cxcl12a*^{t30516} (Green) mutant embryos. (C) Pairwise principal component analysis scatterplots of morphogenetic parameters extracted from the datasets corresponding the tracks in (B). The major difference between control, *neurog1*^{hi1059}, *cxcr4b*^{t26035} and *cxcl12a*^{t30516} mutant embryos (PC1) corresponds to the antero-posterior axis. (D) Clustering analysis of morphogenetic parameters extracted from the datasets corresponding the tracks in (B) and analyzed in (C). One cluster, k1, contains almost exclusively control tracks (Black),

whereas tracks from *neurog1*^{hi1059} (Magenta), *cxcr4b*^{t26035} (Blue) and *cxcl12a*^{t30516} (Green) mutant embryos clustered together in k2, k3 and k4.

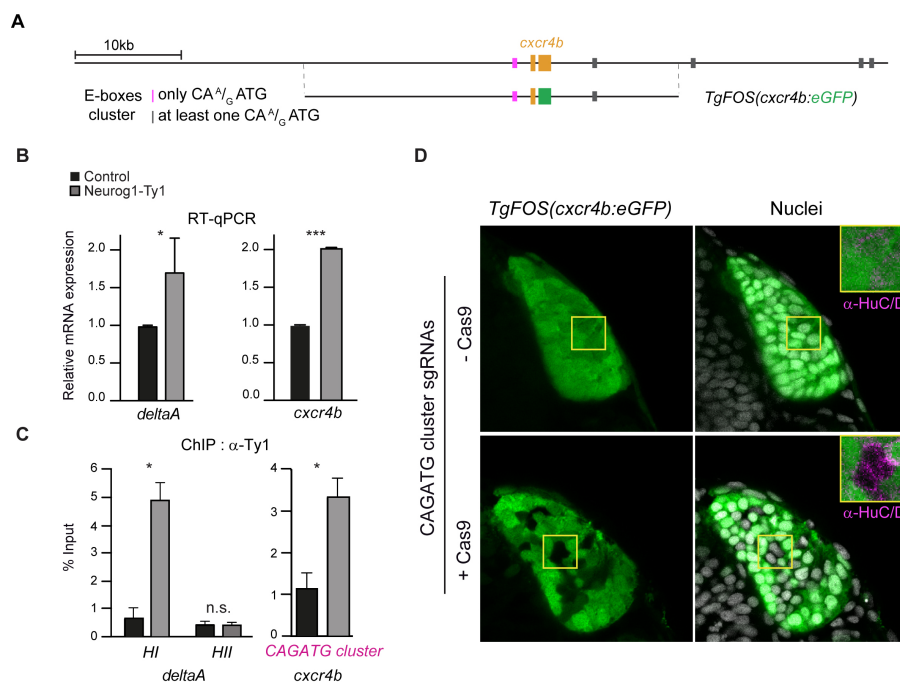


Aguillon et al, Figure 3

Figure 3. *Cxcr4b* is the predominant downstream effector of *Neurog1* during olfactory placode morphogenesis.

(A) *cxcr4b* whole mount *in situ* hybridization at 12, 15 and 18 hpf in control and *neurog1*^{hi1059} mutant embryos. *cxcr4b* expression is dramatically reduced or absent in EON progenitors at 12 and 15 hpf in *neurog1*^{hi1059} mutant embryos (white arrowheads) but from 18 hpf the expression of *cxcr4b* recovers. (B) *cxcl12a* whole mount *in situ* hybridization at 12, 15 and 18 hpf in control and *neurog1*^{hi1059} mutant embryos, in which *cxcl12a* expression is not affected. (C) Tracks showing migration of anterior EONs of control (Black) embryos, *neurog1*^{hi1059} mutant embryos (Magenta), *neurog1*^{hi1059} mutant embryos carrying the Tg(-8.4*neurog1*:*cxcr4b*) transgene (Cyan) and control embryos carrying Tg(-8.4*neurog1*:*cxcr4b*)

(Light Blue). 12 anterior tracks are represented (from 4 embryos). The origin of the tracks has been arbitrarily set to the intersection of the X/Y axis and the early (colored) and late (Grey) phases of migration have been highlighted. **(D)** Mean tracks showing migration of anterior EON of the tracks in **(C)**. **(E)** Pairwise principal component analysis scatterplots of morphogenetic parameters extracted from the datasets corresponding the tracks in **(D)**. The major difference between control, *neurog1^{hi1059}*, and control or *neurog1^{hi1059}* with the rescue transgene (PC1) corresponds to the antero-posterior axis. **(F)** Clustering analysis of morphogenetic parameters extracted from the datasets corresponding the tracks in **(D)** and analyzed in **(E)**. One cluster, k2, contains only *neurog1^{hi1059}* tracks (Magenta), whereas tracks from control (Black), rescue (Cyan) and control/rescue (Light Blue) embryos clustered together in k1, k3 and k4.



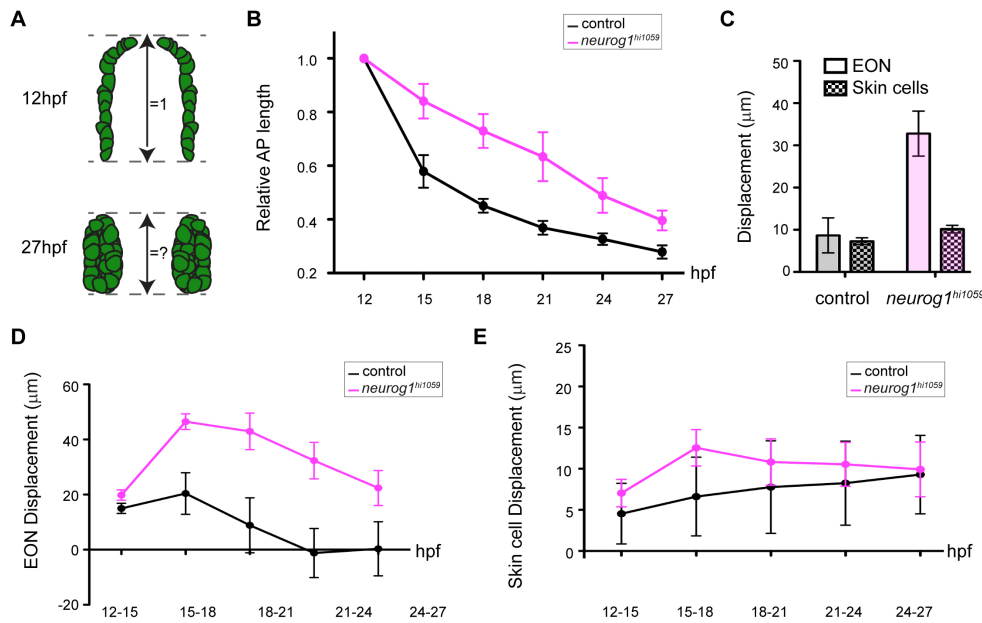
Aguillon et al, Figure 4

Figure 4. Neurog1 directly controls *cxcr4b* expression via an upstream Cis-regulatory module (CRM).

(A) Schematic representation of the *cxcr4b* locus indicating the position of exons of the *cxcr4b* gene (orange) and E-box clusters, which are color-coded depending on the nature of the E-box sequences. Also presented is the approximate position of the genomic sequences found in the *TgFOS(cxcr4b:eGFP)* transgene. **(B)** qPCR analysis of the effect of Neurog1-Ty1 mRNA mis-expression on the relative mRNA levels of the known Neurog1 target gene *deltaA* and *cxcr4b*. A significant increase in expression is detected for both genes. Shown are mean \pm s.e.m, p values are calculated using a two-tailed Student's t-

test, * $p=0.01$, *** $p=0.0001$. **(C)** Chromatin immunoprecipitation (ChIP) using an antibody against Ty1 and chromatin prepared from 15 hpf embryos mis-expressing Neurog1-Ty1 mRNA (Grey). Control (Black) represents ChIP with IgG alone. Shown are mean \pm s.e.m, p values are calculated using a two-tailed Student's t-test, n.s. not significant, * $p=0.01$. **(D)** Single confocal sections of *TgFOS(cxcr4b:eGFP)* embryos at 24 hpf showing eGFP expression in the olfactory placodes, and either HuC/D expression or nuclear labeling (TOPRO). Embryos were injected with an sgRNA pair flanking the E-box containing CRM at the *cxcr4b* locus plus or minus Cas9 as a control. Insets show HuC/D expression in both conditions.

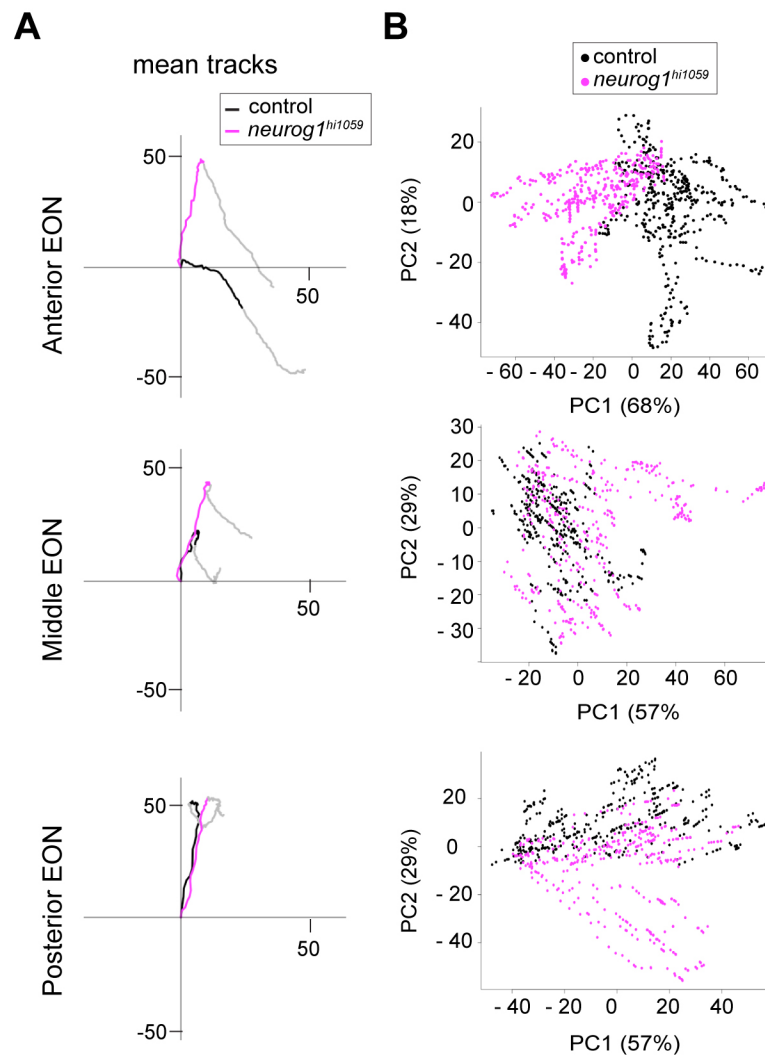
Supplemental Figures



Aguillon et al, Figure S1

Figure S1. *neurog1* mutant embryos display specific defects in olfactory placode development.

(A) Schematic representation of the relative antero-posterior length calculation. Lengths are normalized relative to the 12 hpf antero-posterior length. (B) Graph showing normalized antero-posterior length of the developing olfactory placode in control (Black) and *neurog1^{hi1059}* mutant embryos (Magenta) over time. The mean \pm s.e.m of 12 tracks are represented per condition; 2 cells each from the left and right placodes from 3 embryos for each of the anterior, middle and posterior domains of the developing placode. (C) Histogram showing the global displacement of EON (empty) and skin cells (checkered) of control (Black) and *neurog1^{hi1059}* mutant embryos (Magenta) during olfactory placode development. The mean \pm s.e.m of 12 tracks are represented per condition. (D) Graph showing the global displacement along antero-posterior axis of control (Black) or *neurog1^{hi1059}* mutant (Magenta) EON during five indicated time periods. The mean \pm s.e.m of 36 tracks are represented (12 tracks per embryo and 3 embryos per genotype) per condition. (E) Graph showing the global displacement along antero-posterior axis of control (Black) or *neurog1^{hi1059}* mutant (Magenta) skin cells during five indicated time periods. The mean \pm s.e.m of 36 tracks are represented (12 tracks per embryo and 3 embryos per genotype) per condition.

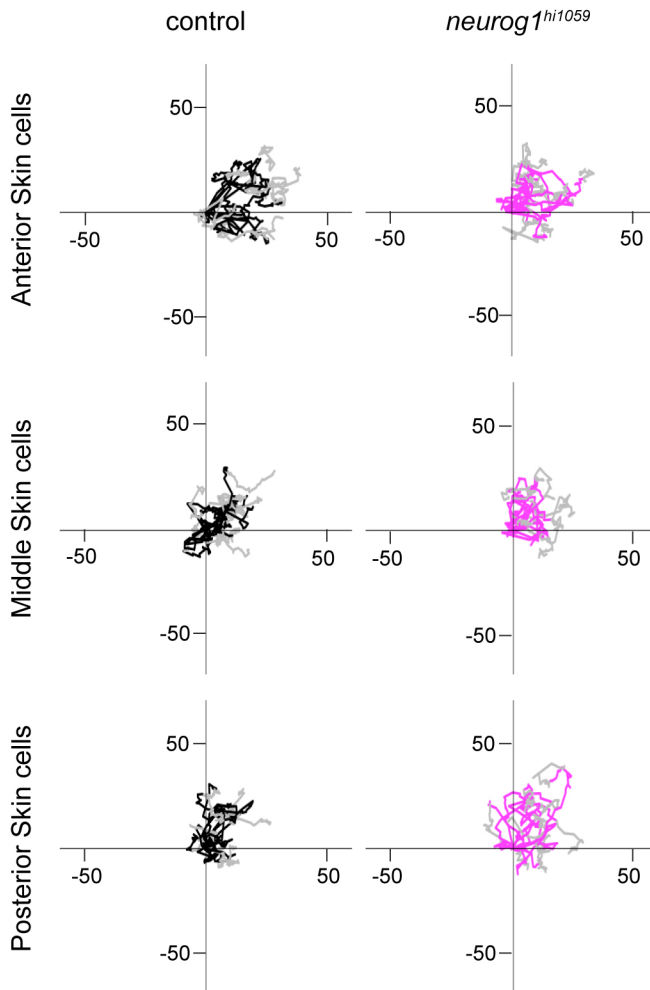


Aguillon et al, Figure S2

Figure S2. Anterior EON population tracks are specifically affected in *neurog1* mutated embryos.

(A) Mean tracks for anterior, middle and posterior EON set of control (Black) or *neurog1^{hi1059}* mutant (Magenta) embryos. 12 tracks are represented (2 cells each from the left and right placodes from 3 embryos) for each region. The origin of the tracks has been arbitrarily set to the intersection of the X/Y axis and the early (colored) and late (Grey) phases of migration have been highlighted. **(B)** Pairwise

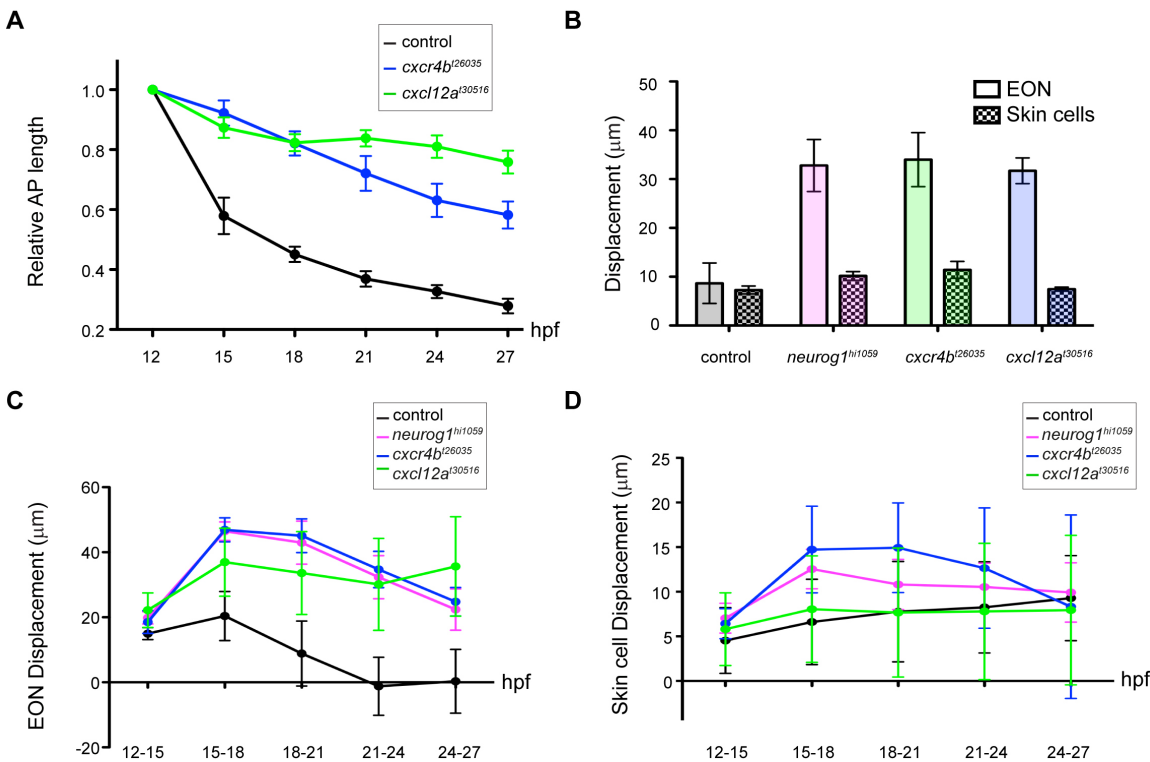
principal component analysis scatterplots of morphogenetic parameters extracted from the datasets corresponding to the tracks in (A).



Aguillon et al, Figure S3

Figure S3. Morphogenetic movements of skin cells in *neurog1^{hi1059}* mutant embryos.

Tracks showing migration of skin cells in control (Black) or *neurog1^{hi1059}* mutant (Magenta) embryos. 12 tracks are represented for cells overlying the anterior, middle and posterior domains of the developing placode. The origin of the tracks has been arbitrarily set to the intersection of the X/Y axis and the early (coloured) and late (Grey) phases of migration have been highlighted. Morphogenetic movements of individual skin cells showed no obvious differences in control versus *neurog1* mutants.

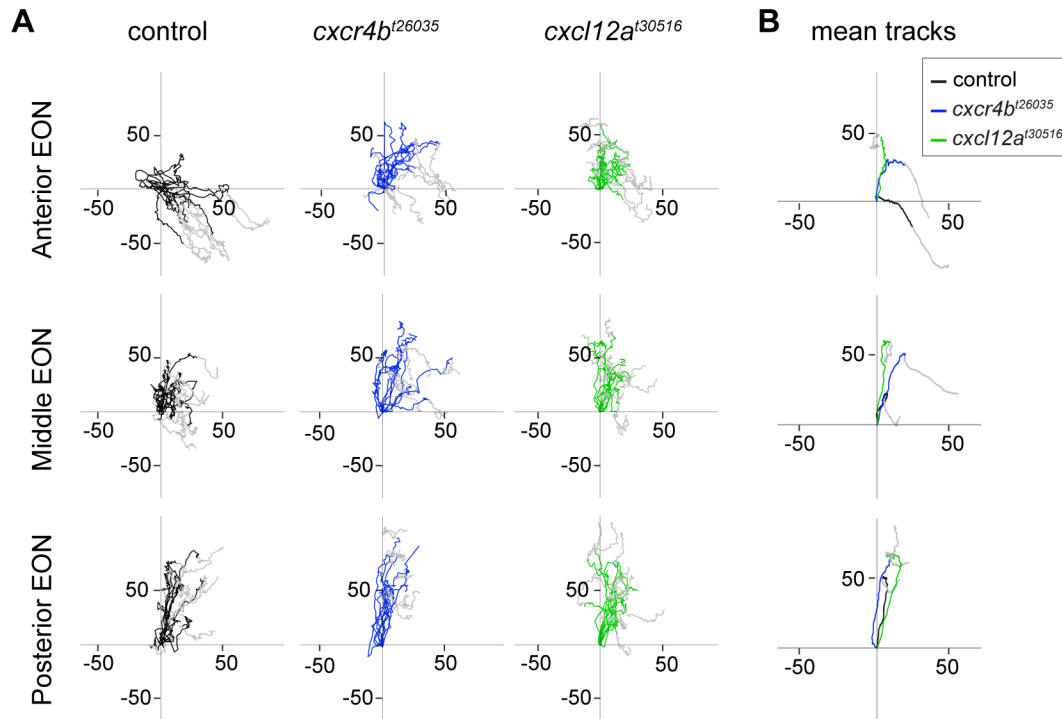


Aguillon et al, Figure S4

Figure S4. Morphogenetic movements of EON are globally affected in *cxcr4b*^{t26035} and *cxcl12a*^{t30516} mutant embryos.

(A) Graph showing normalized antero-posterior length of the developing olfactory placode in control (Black) and *cxcr4b*^{t26035} (Green) and *cxcl12a*^{t30516} (Blue) mutants over time. The mean ± s.e.m of 12 tracks are represented per condition; 2 cells each from the left and right placodes from 3 embryos for each of the anterior, middle and posterior domains of the developing placode. (B) Histogram showing the global displacement of EON (empty) and skin cells (checkered) for control (Black), *neurog1*^{hi1059} (Magenta) *cxcr4b*^{t26035} (Green) and *cxcl12a*^{t30516} (Blue) mutants during olfactory placode development. The mean ± s.e.m of 12 tracks are represented per condition. (C) Graph showing the global displacement along antero-posterior axis of control (Black), *neurog1*^{hi1059} (Magenta) *cxcr4b*^{t26035} (Green) and *cxcl12a*^{t30516} (Blue) EON during five indicated time periods. The mean ± s.e.m of 36 tracks are represented (12 tracks per embryo and 3 embryos per genotype) per condition. (D) Graph showing the

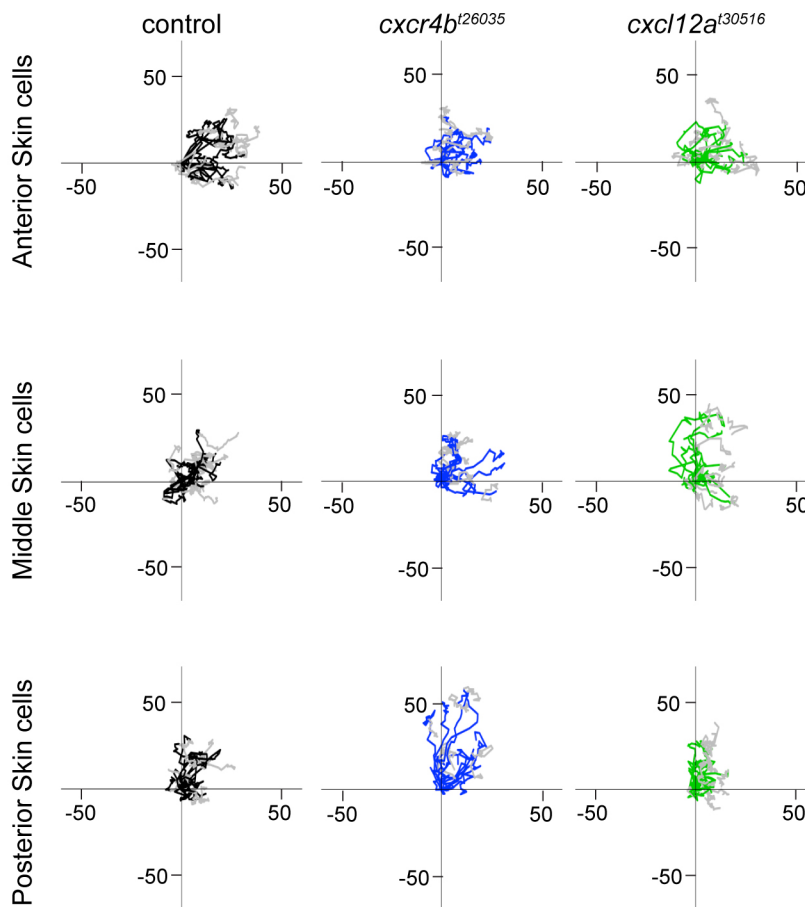
global displacement along antero-posterior axis of control (Black), *neurog1*^{hi1059} (Magenta) *cxcr4b*^{t26035} (Green) and *cxcl12a*^{t30516} (Blue) skin cells during five indicated time periods. The mean \pm s.e.m of 36 tracks are represented (12 tracks per embryo and 3 embryos per genotype) per condition.



Aguillon et al, Figure S5

Figure S5. Morphogenetic parameters in *cxcr4b*^{t26035} and *cxcl12a*^{t30516} mutant embryos.

(A) Tracks showing migration of EON of control (Black), *cxcr4b*^{t26035} (Green) and *cxcl12a*^{t30516} (Blue) embryos. 12 tracks are represented (2 cells each from the left and right placodes from 3 embryos) for each of the anterior, middle and posterior domains of the developing placode. The origin of the tracks has been arbitrarily set to the intersection of the X/Y axis and the early (colored) and late (Grey) phases of migration have been highlighted. (B) Mean tracks for anterior EON of control (Black), *cxcr4b*^{t26035} (Green) and *cxcl12a*^{t30516} (Blue) embryos.



Aguillon et al, Figure S6

Figure S6. Morphogenetic movements of skin cells in *cxcr4b*^{t26035} and *cxcl12a*^{t30516} embryos.

Tracks showing migration of skin cells of control (Black), *cxcr4b*^{t26035} (Green) and *cxcl12a*^{t30516} (Blue) embryos. 12 tracks are represented for cells overlying the anterior, middle and posterior domains of the developing placode. The origin of the tracks has been arbitrarily set to the intersection of the X/Y axis and the early (colored) and late (Grey) phases of migration have been highlighted. Morphogenetic movements of individual skin cells showed no obvious differences in control versus *neurog1* mutants.

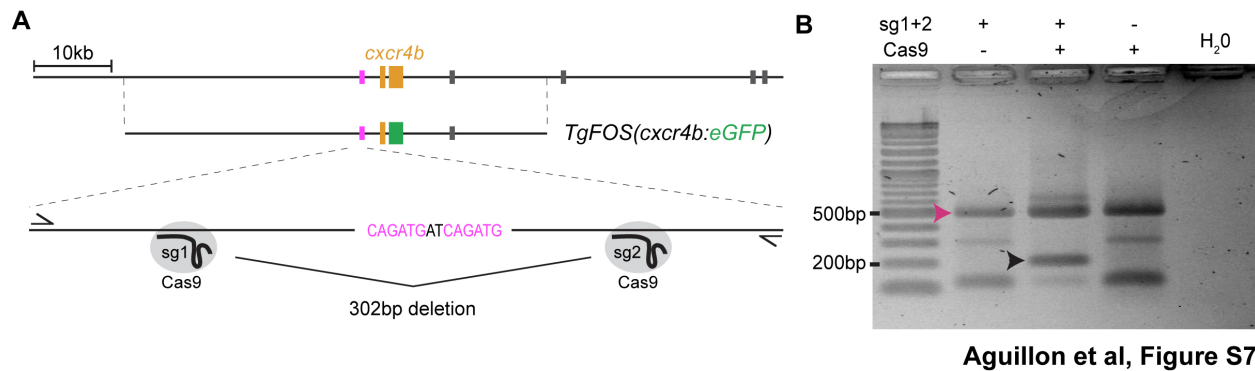


Figure S7. Crispr-Cas9 deletion of the Neurog1-regulated CRM upstream of the *cxcr4b* locus.

(A) Schematic representation of the *cxcr4b* locus indicating the position of exons of the *cxcr4b* gene (orange) and E-box clusters, which are color-coded depending on the nature of the E-box sequences, the approximate position of the genomic sequences found in the *TgFOS(cxcr4b:eGFP)* transgene. Also presented is a schematic representation of the PCR fragment used to genotype potential deletions with the sequence of the E-box cluster. (B) Ethidium bromide stained agarose gel showing the results of PCR genotyping for the induction of deletions of the E-box cluster. The magenta arrowhead shows the 500bp control band. A 200 bps band appears (black arrowhead) when the sgRNA pair is injected with Cas9 but not when the sgRNA pair or Cas9 is injected alone.

References

- Beckers, J., Caron, A., Hrabe de Angelis, M., Hans, S., Campos-Ortega, J. A. and Gossler, A. (2000) Distinct regulatory elements direct delta1 expression in the nervous system and paraxial mesoderm of transgenic mice, *Mech Dev* 95(1-2): 23-34.
- Bertrand, N., Castro, D. S. and Guillemot, F. (2002) Proneural genes and the specification of neural cell types, *Nat Rev Neurosci* 3(7): 517-30.
- Blader, P., Fischer, N., Gradwohl, G., Guillemot, F. and Strahle, U. (1997) The activity of neurogenin1 is controlled by local cues in the zebrafish embryo, *Development* 124(22): 4557-69.
- Blader, P., Plessy, C. and Strahle, U. (2003) Multiple regulatory elements with spatially and temporally distinct activities control neurogenin1 expression in primary neurons of the zebrafish embryo, *Mech Dev* 120(2): 211-8.
- Breau, M. A., Bonnet, I., Stoufflet, J., Xie, J., De Castro, S. and Schneider-Maunoury, S. (2017) Extrinsic mechanical forces mediate retrograde axon extension in a developing neuronal circuit, *Nat Commun* 8(1): 282.
- Burger, A., Lindsay, H., Felker, A., Hess, C., Anders, C., Chiavacci, E., Zaugg, J., Weber, L. M., Catena, R., Jinek, M. et al. (2016) Maximizing mutagenesis with solubilized CRISPR-Cas9 ribonucleoprotein complexes, *Development* 143(11): 2025-37.
- David, N. B., Sapede, D., Saint-Etienne, L., Thisse, C., Thisse, B., Dambly-Chaudiere, C., Rosa, F. M. and Ghysen, A. (2002) Molecular basis of cell migration in the fish lateral line: role of the chemokine receptor CXCR4 and of its ligand, SDF1, *Proc Natl Acad Sci U S A* 99(25): 16297-302.

- Golling, G., Amsterdam, A., Sun, Z., Antonelli, M., Maldonado, E., Chen, W., Burgess, S., Haldi, M., Artzt, K., Farrington, S. et al.** (2002) Insertional mutagenesis in zebrafish rapidly identifies genes essential for early vertebrate development, *Nat Genet* 31(2): 135-40.
- Hans, S. and Campos-Ortega, J. A.** (2002) On the organisation of the regulatory region of the zebrafish deltaD gene, *Development* 129(20): 4773-84.
- Kimmel, C. B., Ballard, W. W., Kimmel, S. R., Ullmann, B. and Schilling, T. F.** (1995) Stages of embryonic development of the zebrafish, *Dev Dyn* 203(3): 253-310.
- Knaut, H., Werz, C., Geisler, R., Nusslein-Volhard, C. and Tubingen Screen, C.** (2003) A zebrafish homologue of the chemokine receptor Cxcr4 is a germ-cell guidance receptor, *Nature* 421(6920): 279-82.
- Kwan, K. M., Fujimoto, E., Grabher, C., Mangum, B. D., Hardy, M. E., Campbell, D. S., Parant, J. M., Yost, H. J., Kanki, J. P. and Chien, C. B.** (2007) The Tol2kit: a multisite gateway-based construction kit for Tol2 transposon transgenesis constructs, *Dev Dyn* 236(11): 3088-99.
- Madelaine, R. and Blader, P.** (2011) A cluster of non-redundant Ngn1 binding sites is required for regulation of deltaA expression in zebrafish, *Dev Biol* 350(1): 198-207.
- Madelaine, R., Garric, L. and Blader, P.** (2011) Partially redundant proneural function reveals the importance of timing during zebrafish olfactory neurogenesis, *Development* 138(21): 4753-62.
- Mattar, P., Britz, O., Johannes, C., Nieto, M., Ma, L., Rebeyka, A., Klenin, N., Polleux, F., Guillemot, F. and Schuurmans, C.** (2004) A screen for downstream effectors of Neurogenin2 in the embryonic neocortex, *Dev Biol* 273(2): 373-89.
- Miyasaka, N., Knaut, H. and Yoshihara, Y.** (2007) Cxcl12/Cxcr4 chemokine signaling is required for placode assembly and sensory axon pathfinding in the zebrafish olfactory system, *Development* 134(13): 2459-68.
- Moreno-Mateos, M. A., Vejnar, C. E., Beaudoin, J. D., Fernandez, J. P., Mis, E. K., Khokha, M. K. and Giraldez, A. J.** (2015) CRISPRscan: designing highly efficient sgRNAs for CRISPR-Cas9 targeting in vivo, *Nat Methods* 12(10): 982-8.
- Nakayama, T., Blitz, I. L., Fish, M. B., Odeleye, A. O., Manohar, S., Cho, K. W. and Grainger, R. M.** (2014) Cas9-based genome editing in *Xenopus tropicalis*, *Methods Enzymol* 546: 355-75.
- Oxtoby, E. and Jowett, T.** (1993) Cloning of the zebrafish krox-20 gene (krx-20) and its expression during hindbrain development, *Nucleic Acids Res* 21(5): 1087-95.
- Revenu, C., Streichan, S., Dona, E., Lecaudey, V., Hufnagel, L. and Gilmour, D.** (2014) Quantitative cell polarity imaging defines leader-to-follower transitions during collective migration and the key role of microtubule-dependent adherens junction formation, *Development* 141(6): 1282-91.
- Shaker, T., Dennis, D., Kurrasch, D. M. and Schuurmans, C.** (2012) Neurog1 and Neurog2 coordinately regulate development of the olfactory system, *Neural Dev* 7: 28.
- Valentin, G., Haas, P. and Gilmour, D.** (2007) The chemokine SDF1a coordinates tissue migration through the spatially restricted activation of Cxcr7 and Cxcr4b, *Curr Biol* 17(12): 1026-31.
- Wardle, F. C., Odom, D. T., Bell, G. W., Yuan, B., Danford, T. W., Wlletta, E. L., Herbolsheimer, E., Sive, H. L., Young, R. A. and Smith, J. C.** (2006) Zebrafish promoter microarrays identify actively transcribed embryonic genes, *Genome Biol* 7(8): R71.
- Whitlock, K. E. and Westerfield, M.** (2000) The olfactory placodes of the zebrafish form by convergence of cellular fields at the edge of the neural plate, *Development* 127(17): 3645-53.